First-principles quantum transport method for disordered nanoelectronics: Disorder-averaged transmission, shot noise, and device-to-device variability

Jiawei Yan,[1,2,3] Shizhuo Wang,[2,4] Ke Xia,[4] and Youqi Ke[1,2,3,*]

[1]*Shanghai Institute of Optics and Fine Mechanics, Chinese Academy of Sciences, Shanghai 201800, China*

[2]*Division of Condensed Matter Physics and Photonic Science, School of Physical Science and Technology, ShanghaiTech University, Shanghai 201210, China*

[3]*University of Chinese Academy of Sciences, Beijing 100049, China*

[4]*The Center for Advanced Quantum Studies and Department of Physics, Beijing Normal University, Beijing 100875, China*

(Received 27 November 2016; revised manuscript received 10 February 2017; published 21 March 2017)

Because disorders are inevitable in realistic nanodevices, the capability to quantitatively simulate the disorder effects on electron transport is indispensable for quantum transport theory. Here, we report a unified and effective first-principles quantum transport method for analyzing effects of chemical or substitutional disorder on transport properties of nanoelectronics, including averaged transmission coefficient, shot noise, and disorder-induced device-to-device variability. All our theoretical formulations and numerical implementations are worked out within the framework of the tight-binding linear muffin tin orbital method. In this method, we carry out the electronic structure calculation with the density functional theory, treat the nonequilibrium statistics by the nonequilbrium Green's function method, and include the effects of multiple impurity scattering with the generalized nonequilibrium vertex correction (NVC) method in coherent potential approximation (CPA). The generalized NVC equations are solved from first principles to obtain various disorder-averaged two-Green's-function correlators. This method provides a unified way to obtain different disorder-averaged transport properties of disordered nanoelectronics from first principles. To test our implementation, we apply the method to investigate the shot noise in the disordered copper conductor, and find all our results for different disorder concentrations approach a universal Fano factor 1/3. As the second test, we calculate the device-to-device variability in the spin-dependent transport through the disordered Cu/Co interface and find the conductance fluctuation is very large in the minority spin channel and negligible in the majority spin channel. Our results agree well with experimental measurements and other theories. In both applications, we show the generalized nonequilibrium vertex corrections play a determinant role in electron transport simulation. Our results demonstrate the effectiveness of the first-principles generalized CPA-NVC for atomistic analysis of disordered nanoelectronics, extending the capability of quantum transport simulation.

DOI: 10.1103/PhysRevB.95.125428

I. INTRODUCTION

In realistic nanoelectronic devices, disorders, such as intentional dopants, surface roughness, interfacial defects, vacancies, impurities, etc., are unavoidable and play important roles in the electron transport. The presence of disorders allows the electron to transport through interchannel scattering and through the disordered impurity states, thus changing the transport into the diffusive regime [1]. Moreover, at nanoscale, devices with different disorder configurations can behave very differently, giving rise to the large device-to-device variability, known as the "random dopant fluctuation" which is an especially important phenomena in the design of nano-FETs [2]. Therefore, quantitative understanding of the disorder effects is of great importance for practical applications. However, theoretical treatment of disorder effects requires statistically averaging the physical properties, namely disorder configurational average which is very difficult. Besides, for nanoscale devices, due to the strong coupling of device properties to the material details and the nonequilibrium characteristics of electron transport, the nanoelectronic device simulations require the accuracy at the atomistic level and the nonequilibrium quantum statistics. Therefore, the effective method to handle disorder average from first principles at nonequilibrium is desirable for quantum transport simulation of the disordered nanoelectronic device.

For first-principles simulation of a quantum transport problem, the widely used method is to combine density functional theory (DFT) [3] with nonequilibrium Green's function (NEGF) theory [4,5], called the NEGF-DFT method [6]. In this method, the electron Hamiltonian is described at the level of DFT, while NEGF formalism is used to populate the electronic structure, accounting for the nonequilibrium quantum statistics. However, presently available NEGF-DFT-based quantum transport tools [6–8] are largely limited to the nanoelectronics with perfect periodicity, because of the prohibitively large cost for the disorder average. Therefore, the analytical method for treating disorder average is required for quantum transport simulations. Presently, the most effective method dealing with disorder is coherent potential approximation (CPA). However, CPA has only been made practical for treating chemical or substitutional disorders under equilibrium condition, but not for the structural disorder (amorphous structure) and systems at nonequilibrium. As an important progress for simulating disordered nanoelectronics, one of the authors, Y. Ke, and his collaborators recently developed a CPA-based nonequilibrium vertex correction (NVC) method in combination with NEGF-DFT to calculate the averaged NEGF, such as $\bar{G}^{<} = \bar{G}^{R}[\Sigma_{ld}^{<} + \Omega_{\mathrm{NVC}}]\bar{G}^{A}$, where $\Sigma_{ld}^{<}$ and

*keyq@shanghaitech.edu.cn

$\Omega_{\rm NVC}$ denote the electrode self-energy and the NVC. In this method, the effects of multiple impurity scattering are taken into account by the NVC at the nonequilibrium density matrix level. The first-principles CPA-NVC method has seen considerable success in applications [9]. However, this method is only limited to compute the averaged I-V characteristics of the device, because the CPA-NVC method only allows one to calculate the average of single $G^<$ which determines the transmission coefficient. However, many other important transport properties of the disordered device require the average of $G^<CG^<$, such as the shot noise, and disorder-induced conductance/current fluctuation. (We also notice that $G^>CG^<$, $G^<CG^>$ are required for the light absorption and emission in the LED or solar cell devices [10].) As we know, the property fluctuation directly measures the device-to-device variability induced by disorders. At nanoscale, due to the limited number of atoms in the device, the change of atoms can induce large changes in the device properties, giving rise to large property fluctuation for disordered devices. Besides, shot noise appears as the current fluctuation in the time domain due to the quantized charge. As known, shot noise contains important information that cannot be obtained from the current/conductance. For example, shot noise can provide the information about unit of transferred effective charge [11], reflects the electron-electron correlation during transport, detects the open channels in a disordered conductors [12], and even distinguishes particles from waves [13]. However, due to the lack of an effective method to do disorder average, the device-to-device variability and shot noise from first-principles simulations are rarely reported in the literature for disordered nanoelectronics [14–17]. To solve the problem, the authors J. Yan and Y. Ke recently reported a generalized CPA-NVC formalism to compute the average of various two-GF correlators in a unified way, and tested the method with a simple tight-binding Hamiltonian [18].

In this paper, we report the first-principles implementation of the generalized CPA-NVC method, to extend the capability of quantum transport simulations of disordered nanoelectronics. We reformulate the generalized CPA-NVC formalism within the well-established first-principles framework of the tight-binding linear muffin tin orbital method (TB-LMTO). The generalized nonequilibrium vertex correction (GNVC) equations are solved from first principles to obtain various disorder averaged two-GF correlators. As important results, various transport properties of disordered nanoelectronics can be obtained without using any phenomenological parameters. As applications, we investigated the shot noise in the disordered copper metal conductor and the spin-dependent device-to-device variability in the transport through the disordered Cu/Co interface. Our results agree well with the experiments and other theories, providing strong tests to the effectiveness of the generalized CPA-NVC formalism and its first-principles implementation. We have shown the inclusion of GNVCs is essential for transport simulation of disordered nanoelectronics.

The rest of the paper is organized as follows. In Sec. II, we introduce the NEGF-based quantum transport formalism in the TB-LMTO method, and write various quantum transport properties as well as the nonequilibrium density matrix in terms of an auxiliary Green's function. In Sec. III, we apply the generalized CPA-NVC formalism to formulate the average of the single auxiliary GF and various two-auxiliary-GF correlators. In Sec. IV, we present the computation of the disordered averaged transport quantities, including transmission coefficients, shot noise, and the transmission fluctuation, to realize the first-principles simulation of disordered nanoelectronics. In Sec. V, we apply the present implementation to investigate the shot noise for the disordered copper conductor and disorder-induced device-to-device variability for the spin-dependent transport through the disordered Cu/Co interface, and compare our results with experimental measurements and other theories. Finally, we conclude in Sec. VI and provide additional information in Appendixes A–E.

II. NEGF FORMALISM IN TB-LMTO FOR QUANTUM TRANSPORT

The method of tight-binding (TB) linearized muffin-tin orbital (LMTO) in combination with atomic sphere approximation (ASA) [19–21] has been well established for first-principles simulation of electronic structure of condensed matters. This method separates the atomic potential aspects of a material from the structural aspects, and can be easily incorporated with the Green's function formalism. In the following, we introduce the TB-LMTO method and its implementation for nonequilibrium quantum transport simulation.

A. Tight-binding linearized MTO method

For a material system, the space can be partitioned into atomic spheres and an interstitial region. In such a muffin-tin (MT) geometry, the system potential can be represented in the MT approximation,

$$V_{\rm MT} = V_{\rm MTZ} + \sum_{\mathbf{R}} V_{{\rm MT},\mathbf{R}}(r_{\mathbf{R}}), \tag{1}$$

on which the TB-LMTO is based. In the above equation, $V_{\rm MTZ}$ is a constant potential in the interstitial region and $V_{{\rm MT},\mathbf{R}}$ is a spherically symmetric potential inside the MT sphere centered on the site $\mathbf{R}$ [19]. The TB-LMTO is constructed to provide a very efficient approach to solve the Schrödinger equation containing the MT potential in Eq. (1). Since the construction details of the TB-LMTO have been well included in the literature [19–21], we here only provide the major results and approximations of this method. TB-LMTOs have a general form given as

$$|\chi^\alpha\rangle^\infty = |\phi> (1 + o^\alpha h^\alpha) + |\dot{\phi}\rangle h^\alpha + |K^\alpha\rangle^i / N^\alpha, \tag{2}$$

where $h^\alpha \equiv -\sqrt{\dot{P}^\alpha}(P^\alpha - S^\alpha)\sqrt{\dot{P}^\alpha}$. In the above equation, α denotes the screening constant; $\phi_{\mathbf{R}lL} = \phi_{\mathbf{R}l}(r_{\mathbf{R}})Y_L(\hat{r}_R)$ is the partial wave inside the MT sphere at $\mathbf{R}$; $|K^\alpha\rangle^i$ is the screened envelop function inside the interstitial region; P^α and N^α are the potential and normalization functions introduced to ensure the continuity of basis functions at the sphere boundaries; the quantity o^α is chosen to satisfy the linearization condition; and S^α is the screened structure constant. To avoid the integration in the interstitial region, atomic sphere approximation (ASA) [21] is applied to fill the entire space with overlapping atomic spheres. As an important result, the interstitial contribution to the TB-LMTO can be neglected, thus the TB-LMTO

changes to $|\chi^{\alpha}_{\rm ASA}>^{\infty}=|\phi>(1+o^{\alpha}h^{\alpha})+|\dot{\phi}>h^{\alpha}$ in ASA. By transforming to the nearly orthogonal representation, one can obtain the final nearly orthogonal TB-LMTO in ASA as follows:

$$\left|\chi^{\rm orth}_{\rm ASA}\right\rangle^{\infty}=|\phi\rangle+|\dot{\phi}\rangle h^{\alpha}(1+o^{\alpha}h^{\alpha})^{-1}. \tag{3}$$

With the above basis functions, the Hamiltonian matrix of the material system can be expressed as

$$\begin{aligned} H^{\rm orth}_{\rm ASA} &= {}^{\infty}\langle\chi^{\rm orth}_{\rm ASA}|-\tfrac{1}{2}\nabla^2+V_{\rm MT}|\chi^{\rm orth}_{\rm ASA}\rangle^{\infty} \\ &= \epsilon_v+h^{\alpha}(1+o^{\alpha}h^{\alpha})^{-1}, \end{aligned} \tag{4}$$

where ϵ_v is the linear expansion energy center at which the partial wave $\phi_{\mathbf{R}l}$ is solved. It should be noted that the Hamiltonian matrix in Eq. (4) can be easily constructed by solving the local Schrödinger equation for the partial waves within each atomic sphere. The simple and analytical form of the Hamiltonian matrix in TB-LMTO-ASA provides great convenience for further analytical derivation of NEGF formalism for quantum transport.

B. Quantum transport in TB-LMTO

Here, we consider an operating two-probe electronic device as shown in Fig. 1 with current flow from one side to the other induced by the applied bias. (We assume $\mu_L>\mu_R$, where $\mu_{L/R}$ denotes the chemical potential of the left/right electrode.)

To deal with such a nonequilibrium quantum transport problem, the most general and rigorous theoretical framework is provided by the nonequilbrium Green's function (NEGF) theory [5,22–24]. The NEGF theory provides a unified way to treat quantum transport problem with various interactions contained in self-energies, such as interactions with electrodes, phonon/photon, random impurities, etc.. The key idea of the NEGF theory is the closed time contour and the associated contour order. The contour-ordered quantities, such as Green's function, self-energies, can be usually expressed with the Keldysh's rotation, thus can be represented by the Keldysh's 2-by-2 matrix [5,25,26],

$$Q=\begin{pmatrix} Q^R & Q^K \\ 0 & Q^A \end{pmatrix}. \tag{5}$$

Here, Q^R, Q^A, and Q^K are the retarded, advanced, and Keldysh's components of the contour-ordered quantity Q, and they satisfy $Q^R=[Q^A]^{\dagger}$ and $Q^K=-[Q^K]^{\dagger}$ and are linearly independent. The linear combination of Q^R, Q^A, and Q^K can directly give other real-time quantities, such as $Q^<$, $Q^>$, Q^t, and $Q^{\bar{t}}$ [18]. For example, the important quantities "Lesser" Green's function $G^<=\frac{1}{2}(G^K-G^R+G^A)$.

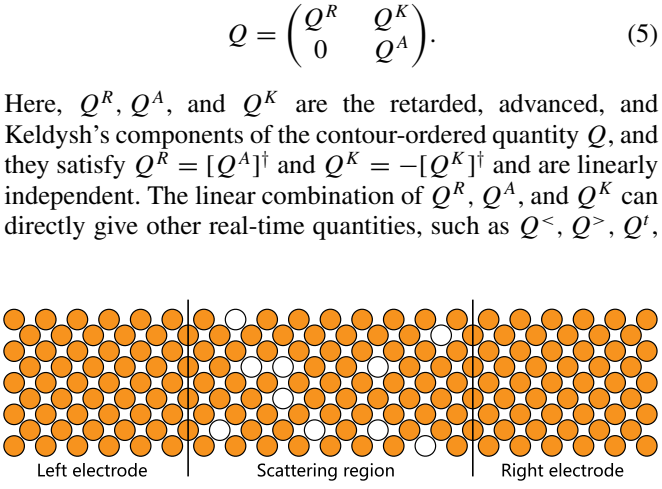

FIG. 1. Schematic illustration of a two-probe device. The central scattering region containing atomic disorders (white spheres) is sandwiched by the left and right semi-infinite electrodes. Applying an external bias drives the central device out of equilibrium.

In the TB-LMTO method, the contour-ordered physical Green's function of the interested central device region (usually G is called physical Green's function to distinguish from the auxiliary Green's function g in the following) can be written as

$$G(z)=-\frac{1}{2}\frac{\ddot{P}^{\alpha}(z)}{\dot{P}^{\alpha}(z)}+\sqrt{\dot{P}^{\alpha}(z)}\,\mathrm{g}^{\alpha}(z)\sqrt{\dot{P}^{\alpha}(z)}, \tag{6}$$

with the auxiliary Green's function defined as [19]

$$\mathrm{g}^{\alpha}(z)=\left[P^{\alpha}(z)-S^{\alpha}-\Sigma^{\alpha}_{ld}\right]^{-1}. \tag{7}$$

Here, the potential function P^{α} (site-diagonal) specifies the atomic species on the lattice site, the screened structure constant S^{α} contains the geometric information of the device, and Σ^{α}_{ld} is the auxiliary self-energy describing the coupling to the electrodes, such as $\Sigma^{\alpha}_{ld}=\Sigma^{\alpha}_{L}+\Sigma^{\alpha}_{R}$ for a two-probe device. $\dot{P}^{\alpha}(z)$ and $\ddot{P}^{\alpha}(z)$ refer to the first- and second-order energy derivatives of $P^{\alpha}(z)$. Superscript α denotes the screened representation. All the quantities in Eqs. (6) and (7) are defined in the Keldysh's matrix representation in Eq. (5) for treating the nonequilibrium quantum transport problem. Since Eq. (6) provides a simple connection between the physical and auxiliary Green's functions, we will focus on the computation of $\mathrm{g}^{\alpha}(z)$ in the following.

To evaluate g^{α}, we can define the unperturbed Green's function $\mathrm{g}^{\alpha,0}$ for the central region without coupling to the left and right electrodes. Then, g^{α} in Eq. (7) can be rewritten as the Dyson equation,

$$\mathrm{g}^{\alpha}=\mathrm{g}^{\alpha,0}+\mathrm{g}^{\alpha,0}\Sigma^{\alpha}_{ld}\mathrm{g}^{\alpha}. \tag{8}$$

Replacing g^{α} and Σ^{α} in Eq. (8) with the Keldysh's matrices leads to

$$\mathrm{g}^{\alpha,R}=\left(P^{\alpha,R}-S^{\alpha,R}-\Sigma^{\alpha,R}_{ld}\right)^{-1}, \tag{9}$$

$$\mathrm{g}^{\alpha,K}=\mathrm{g}^{\alpha,R}\Sigma^{\alpha,K}_{ld}\mathrm{g}^{\alpha,A}, \tag{10}$$

where Eq. (10) is obtained by dropping the boundary term $(I+\mathrm{g}^{\alpha,R}\Sigma^{\alpha,R})\mathrm{g}^{\alpha,0,K}(I+\Sigma^{\alpha,A}\mathrm{g}^{\alpha,A})$ because it is zero for the device in the steady state considered here [1]. Since the electrodes are in the equilibrium state, according to the fluctuation-dissipation theorem, we have $\Sigma^{\alpha,K}=i(2f_L-1)\Gamma^{\alpha}_{L}+i(2f_R-1)\Gamma^{\alpha}_{R}$, where $\Gamma^{\alpha}_{L/R}=i(\Sigma^{\alpha,R}_{L/R}-\Sigma^{\alpha,A}_{L/R})$, and $f_{L/R}$ are the Fermi-Dirac distribution functions of the left/right electrodes, respectively. The "lesser" GF in TB-LMTO can be obtained as $G^<=\sqrt{\dot{P}^{\alpha}}\mathrm{g}^{\alpha,<}\sqrt{\dot{P}^{\alpha}}$, where $\mathrm{g}^{\alpha,<}=(-\mathrm{g}^{\alpha,R}+\mathrm{g}^{\alpha,A}+\mathrm{g}^{\alpha,K})/2=\mathrm{g}^{\alpha,R}\Sigma^{\alpha,<}\mathrm{g}^{\alpha,A}$ [8,18,27,28], providing the nonequilibrium density matrix of the device as $iG^<$. Consequently, in combination with density functional theory, the nonequilibrium electronic structure can be calculated self-consistently with the NEGF theory.

For the quantum transport, the I-V curve of the device can be given by the Landauer-Büttiker formula [1],

$$I=\frac{e}{h}\int \mathrm{Tr}[\hat{T}(E)](f_L-f_R)dE. \tag{11}$$

Here, e is the elementary charge, h is the Planck constant, and $\hat{T}(E)$ is the transmission operator at energy E, which in

TB-LMTO is given by $\hat{T} = \mathrm{g}^{\alpha,R}\Gamma_L^\alpha \mathrm{g}^{\alpha,A}\Gamma_R^\alpha$. For simplicity, we consider $f_L = 1$ and $f_R = 0$ at zero temperature, and then $\hat{T}$ can be rewritten as $\hat{T} = -i\mathrm{g}^{\alpha,<}\Gamma_R^\alpha$ [8,27]. Shot noise can also be expressed in terms of $\hat{T}(E)$ [29],

$$S = \frac{2e^2}{h}\int_{\mu_R}^{\mu_L} \mathrm{Tr}[\hat{T}(E) - \hat{T}^2(E)]dE. \tag{12}$$

A very useful quantity related to shot noise is Fano factor $F = S/2eI$ describing the noise deviating from a Poisson noise $S_{\mathrm{Poisson}} = 2eI$ [30,31].

The formulation above is for a system with specific atomic configuration. However, for disordered electronic device, transport properties are random quantities and thus must be averaged over all the possible disorder configurations to be physically meaningful, such as the averaged nonequilibrium density matrix, the averaged $\langle\hat{T}\rangle$ and $\langle\hat{T}^2\rangle$ that give the averaged current and shot noise. To do these, it is required to do the disorder average to $\mathrm{g}^{\alpha,<}$ which is the product of $\mathrm{g}^{\alpha,R}$ and $\mathrm{g}^{\alpha,A}$, and the product of two $\mathrm{g}^{\alpha,<}$s. Furthermore, for disordered nanodevices, it is important to measure the disorder-induced device-to-device variability. Hence, we need to calculate the transmission fluctuation, defined as $\delta T = \sqrt{\langle T^2\rangle - \langle T\rangle^2}$, where $T = \mathrm{Tr}[\hat{T}]$ is the transmission coefficient. To calculate $\langle T^2\rangle$, we are required to average the product of two $\mathrm{g}^{\alpha,<}$s. Therefore, for quantum transport simulation of disordered nanoelectronics, the central task is to compute the disorder-averaged two-GF correlators mentioned above. In the following, we will formulate the generalized CPA-NVC method in TB-LMTO to provide an effective method to compute the average of various two-GF correlators from first principles.

III. GENERALIZED CPA-NVC FORMALISM IN TB-LMTO

In this section, we formulate the generalized CPA-NVC method in TB-LMTO to compute the disorder-averaged two-GF correlators, such as $\langle \mathrm{g}^{\alpha,R} c \mathrm{g}^{\alpha,A}\rangle$ and $\langle \mathrm{g}^{\alpha,<} c \mathrm{g}^{\alpha,<}\rangle$, in which c is a constant matrix independent of disorder configurations. The central idea of CPA is to construct an effective coherent medium, by making sure the configurationally averaged GF of the disordered system $\langle \mathrm{g}^\alpha\rangle$ equals to the Green's function of the effective medium $\bar{\mathrm{g}}^\alpha$ [32,33]. To quantitatively describe this approximation, we can introduce a coherent potential function $\mathcal{P}^\alpha$ to characterize effective atom in the coherent medium, and then the corresponding auxiliary GF is given by

$$\bar{\mathrm{g}}^\alpha = \left(\mathcal{P}^\alpha - S^\alpha - \Sigma_{ld}^\alpha\right)^{-1}. \tag{13}$$

For a specific disordered system, g^α in Eq. (7) can be expressed in terms of $\bar{\mathrm{g}}^\alpha$ by using

$$\mathrm{g}^\alpha = \bar{\mathrm{g}}^\alpha + \bar{\mathrm{g}}^\alpha T^\alpha \bar{\mathrm{g}}^\alpha, \tag{14}$$

where $T^\alpha \equiv [1 - (\mathcal{P}^\alpha - P^\alpha)\bar{\mathrm{g}}^\alpha]^{-1}(\mathcal{P}^\alpha - P^\alpha)$ containing all the scattering information. We can rewrite $T^\alpha = \sum_{\mathbf{R}} Q_{\mathbf{R}}^\alpha$ and $Q_{\mathbf{R}}^\alpha = t_{\mathbf{R}}^\alpha(1 + \bar{\mathrm{g}}^\alpha \sum_{\mathbf{R}'\neq\mathbf{R}} Q_{\mathbf{R}'}^\alpha)$ where $t_{\mathbf{R}}^\alpha \equiv [1 - (\mathcal{P}_{\mathbf{R}}^\alpha - P_{\mathbf{R}}^\alpha)\bar{\mathrm{g}}^\alpha]^{-1}(\mathcal{P}_{\mathbf{R}}^\alpha - P_{\mathbf{R}}^\alpha)$ represents a single-site scatter, and $Q_{\mathbf{R}}^\alpha$ denotes the strength of a scatter at site $\mathbf{R}$. By applying the relation $\langle \mathrm{g}^\alpha\rangle = \bar{\mathrm{g}}^\alpha$ to Eq. (14), we can obtain the CPA condition that

$$\langle T^\alpha\rangle = 0. \tag{15}$$

Usually, to make the CPA practical, an additional single-site approximation (SSA) [34] is applied, namely $\langle Q_{\mathbf{R}}^\alpha\rangle = \langle t_{\mathbf{R}}^\alpha\rangle(1 - \bar{\mathrm{g}}^\alpha \sum_{\mathbf{R}'\neq\mathbf{R}}\langle Q_{\mathbf{R}'}^\alpha\rangle)$ which neglects the correlations between the successive scattering events. After SSA, the single-site CPA condition can be written as

$$\langle t_{\mathbf{R}}^\alpha\rangle = 0. \tag{16}$$

Combining Eq. (13) with Eq. (16), $\mathcal{P}^\alpha$ can be solved self-consistently to obtain $\langle \mathrm{g}^\alpha\rangle$.

For the product of two GFs, the generalized NVC provides a way to average such quantity like $\langle \mathrm{g}^\alpha C \mathrm{g}^\alpha\rangle$, where C is a disorder-independent constant 2-by-2 matrix containing the constant c as the matrix element [18,35]. Substituting Eq. (14) into $\langle \mathrm{g}^\alpha C \mathrm{g}^\alpha\rangle$ and applying CPA condition Eq. (15) leads to

$$\langle \mathrm{g}^\alpha C \mathrm{g}^\alpha\rangle = \bar{\mathrm{g}}^\alpha C \bar{\mathrm{g}}^\alpha + \bar{\mathrm{g}}^\alpha \Omega^\alpha \bar{\mathrm{g}}^\alpha, \tag{17}$$

where $\Omega^\alpha \equiv \langle T^\alpha \bar{\mathrm{g}}^\alpha C \bar{\mathrm{g}}^\alpha T^\alpha\rangle$ is called the generalized NVC, containing not only effects of multiple impurity scattering, but also the nonequilibrium quantum statistics. SSA is applied again, and then one can obtain $\Omega^\alpha = \sum_{\mathbf{R}} \Omega_{\mathbf{R}}^\alpha$, where $\Omega_{\mathbf{R}}^\alpha = \langle Q_{\mathbf{R}}^\alpha \bar{\mathrm{g}}^\alpha C \bar{\mathrm{g}}^\alpha Q_{\mathbf{R}}^\alpha\rangle$ are determined by a linear equation,

$$\Omega_{\mathbf{R}}^\alpha = \left\langle t_{\mathbf{R}}^\alpha [\bar{\mathrm{g}}^\alpha C \bar{\mathrm{g}}^\alpha]_{\mathbf{R}\mathbf{R}} t_{\mathbf{R}}^\alpha\right\rangle + \sum_{\mathbf{R}'\neq\mathbf{R}} \left\langle t_{\mathbf{R}}^\alpha \bar{\mathrm{g}}_{\mathbf{R}\mathbf{R}'}^\alpha \Omega_{\mathbf{R}'}^\alpha \bar{\mathrm{g}}_{\mathbf{R}'\mathbf{R}}^\alpha t_{\mathbf{R}}^\alpha\right\rangle. \tag{18}$$

Note that the quantities in the above equation are all in the 2-by-2 matrix representation, such as g^α and t^α is in the form of Keldysh's representation of Eq. (5). With the four different choices of the capitalized C matrix [18], we can obtain nine different GNVCs $\Omega^{\alpha,XY}(X,Y = R,A,K)$ and associated nine equations to compute the configurational average of the pairwise combination of $\mathrm{g}^X c \mathrm{g}^Y$, such as Eqs. (A1)–(A9). (Appendix A lists the major results of the generalized CPA-NVC formalism in the TB-LMTO method.) As an important result, the average of any two-GF correlators can be easily obtained as a linear combination of $\langle \mathrm{g}^X c \mathrm{g}^Y\rangle$, such as $\langle \mathrm{g}^< c \mathrm{g}^<\rangle$ given in Eq. (A19). Here, we want to mention that, before solving the nine vertex corrections, the averaged Keldysh's GF, $\bar{\mathrm{g}}^K = \langle \mathrm{g}^R \Sigma^K \mathrm{g}^A\rangle$, is calculated by including the vertex correction which satisfies Eq. (A11). It should be also mentioned that each $\langle \mathrm{g}^X c \mathrm{g}^Y\rangle$ contains a coherent part and vertex correction part(s), and the vertex correction part(s) accounts for the effects of multiple impurity scattering. Given the quantity c, the nine GNVCs can be, in general, obtained by solving linear equations Eqs. (A10)–(A18) in the order from top to down. However, the different content of the c matrix can give different complexity in calculating the related physical quantity, such as the computation of the averaged shot noise and transmission fluctuation introduced in the following.

IV. APPLICATION TO DISORDERED NANOELECTRONICS

As mentioned in Sec. III, for disordered nanoelectronics, it is required to compute the disorder-averaged quantities, such as transmission coefficient, shot noise or even the transmission fluctuation, for which we need to compute the averaged $\mathrm{Tr}[\langle\hat{T}\rangle]$, $\mathrm{Tr}[\langle\hat{T}^2\rangle]$, and $\langle(\mathrm{Tr}[\hat{T}])^2\rangle$. In this section, we present

the implementation of the generalized CPA-NVC method to calculate these important transport quantities. For the ease of reading, we will omit the superscript α in the rest of this paper.

A. Averaged transmission

From Sec. II, we know the averaged transmission coefficient $\langle T\rangle = \mathrm{Tr}[\langle \mathrm{g}^R\Gamma_L \mathrm{g}^A\rangle\Gamma_R]$ contains the average over the product of two GFs g^R and g^A. From Eq. (A2), we can see that the computation of $\langle T\rangle$ involves a coherent part and a vertex correction part, namely

$$\langle T\rangle = \mathrm{Tr}[\bar{\mathrm{g}}^R\Gamma_L\bar{\mathrm{g}}^A\Gamma_R] + \mathrm{Tr}[\bar{\mathrm{g}}^R\Omega^{RA}\bar{\mathrm{g}}^A\Gamma_R], \tag{19}$$

where the vertex correction Ω^{RA} can be solved from the linear equation Eq. (A11) which is one of the simplest compared to other GNVC equations. Since the translational invariance is restored after the average, we do lattice Fourier transformation and Eq. (19) can be rewritten as,

$$\langle T\rangle = \sum_{\mathbf{T}}\int_\Lambda \mathrm{Tr}[\bar{\mathrm{g}}^R(\mathbf{k})\Gamma_L(\mathbf{k})\bar{\mathrm{g}}^A(\mathbf{k})\Gamma_R(\mathbf{k})] + \sum_{\mathbf{T}}\int_\Lambda \mathrm{Tr}[\bar{\mathrm{g}}^R(\mathbf{k})\Omega^{RA}\bar{\mathrm{g}}^A(\mathbf{k})\Gamma_R(\mathbf{k})], \tag{20}$$

where $\mathbf{T}$ and $\mathbf{k}$ are the translational vector and the k point in the first Brillouin zone (BZ), denoted as Λ. It should be mentioned that, in the coherent part (the first term in the above equation), electron transports through the device by conserving the $\mathbf{k}$, the same as the perfect device. The presence of disorders gives rise to the nonzero Ω, thus the vertex correction part in Eq. (20) to account for the effects of interchannel scattering in which $\mathbf{k}$ is not conserved (this is prohibited in the perfect device). The mathematical structure of Ω^{RA} in the above equation is very similar to that of the GNVCs involved in $\langle\hat{T}^2\rangle$ that we will discuss in the next subsection.

B. Averaged shot noise

After obtaining the averaged transmission $\langle T\rangle$, calculating the averaged shot noise still requires the average of $\mathrm{Tr}[\langle\hat{T}^2\rangle]$. From Sec. II, we can rewrite $\langle\hat{T}^2\rangle = -\langle \mathrm{g}^<\Gamma_R\mathrm{g}^<\rangle\Gamma_R$ which contains the average over the product of two $\mathrm{g}^<$s. From Eq. (A19), we can see the averaged $\langle \mathrm{g}^<\Gamma_R\mathrm{g}^<\rangle$ can be calculated by the linear combination of the averaged nine two-GF correlators, namely $\langle \mathrm{g}^X\Gamma_R\mathrm{g}^Y\rangle$,$(X,Y = R,A,K)$. According to Eqs. (A1)–(A9), each $\langle \mathrm{g}^X\Gamma_R\mathrm{g}^Y\rangle$ takes a similar form, containing a coherent part plus vertex correction terms. Here we take the RR part of $\mathrm{Tr}[\langle\hat{T}^2\rangle]$ as an example. According to Eq. (A1), we obtain

$$\mathrm{Tr}[\langle\hat{T}^2\rangle]^{(RR)} = \mathrm{Tr}[\bar{\mathrm{g}}^R\Gamma_R\bar{\mathrm{g}}^R\Gamma_R] + \mathrm{Tr}[\bar{\mathrm{g}}^R\Omega^{RR}\bar{\mathrm{g}}^R\Gamma_R]. \tag{21}$$

With lattice Fourier transform, we obtain

$$\mathrm{Tr}[\langle\hat{T}^2\rangle]^{(RR)} = \sum_{\mathbf{T}}\int_\Lambda \mathrm{Tr}[\bar{\mathrm{g}}^R(\mathbf{k})\Gamma_R(\mathbf{k})\bar{\mathrm{g}}^R(\mathbf{k})\Gamma_R(\mathbf{k})] + \sum_{\mathbf{T}}\int_\Lambda \mathrm{Tr}[\bar{\mathrm{g}}^R(\mathbf{k})\Omega^{RR}\bar{\mathrm{g}}^R(\mathbf{k})\Gamma_R(\mathbf{k})], \tag{22}$$

by using the relations $\Omega^{RR}_{\mathbf{BT}} = \Omega^{RR}_{\mathbf{B}}$ and $\Omega^{RR} = \sum_{\mathbf{BT}}\Omega^{RR}_{\mathbf{BT}}$ in SSA ($\mathbf{B}$ is the basis in a unit cell). Here $\Omega^{RR}_{\mathbf{B}}$ is given by Eq. (A10). After lattice Fourier transform, we obtain the equation for $\Omega^{RR}_{\mathbf{B}}$ in the following form:

$$\Omega^{RR}_{\mathbf{B}} = \left\langle t_{\mathbf{B}}\int_\Lambda [\bar{\mathrm{g}}^R(\mathbf{k})\Gamma_R(\mathbf{k})\bar{\mathrm{g}}^R(\mathbf{k})]_{\mathbf{BB}}t_{\mathbf{B}}\right\rangle - \left\langle t_{\mathbf{B}}\bar{\mathrm{g}}^R_{\mathbf{BB}}\Omega^{RR}_{\mathbf{B}}\bar{\mathrm{g}}^R_{\mathbf{BB}}t_{\mathbf{B}}\right\rangle + \left\langle t_{\mathbf{B}}\sum_{\mathbf{B}'}\int_\Lambda \bar{\mathrm{g}}^R_{\mathbf{BB}'}(\mathbf{k})\Omega^{RR}_{\mathbf{B}'}\bar{\mathrm{g}}^R_{\mathbf{B}'\mathbf{B}}(\mathbf{k})t_{\mathbf{B}}\right\rangle, \tag{23}$$

which can be solved by the standard linear algebra. It should be emphasized that one has to solve the GNVC equations in the order from Eq. (A10) to Eq. (A18), so that one solves for only one unknown Ω^{XY} each time. Appendix B provides some more details about Eqs. (22) and (23). After obtaining all the required GNVCs, the $\mathrm{Tr}[\langle\hat{T}^2\rangle]$ can be computed from first principles to obtain the averaged shot noise for disordered nanoelectronics.

C. Transmission fluctuation

The transmission fluctuation induced by disorder is defined as $\delta T = \sqrt{\langle T^2\rangle - \langle T\rangle^2}$. According to Sec. II, we have

$$\langle T^2\rangle = -\langle \mathrm{Tr}[\mathrm{g}^<\Gamma_R]\cdot\mathrm{Tr}[\mathrm{g}^<\Gamma_R]\rangle. \tag{24}$$

To compute $\langle T^2\rangle$, we write

$$\Gamma_{\mathbf{B}_1\mathbf{T}_1,\mathbf{B}_2\mathbf{T}_2} = \int_\Lambda \Gamma_{\mathbf{B}_1,\mathbf{B}_2}(\mathbf{k})e^{-i\mathbf{k}\cdot(\mathbf{T}_2-\mathbf{T}_1)}, \tag{25}$$

where the subscript R has been omitted. By introducing the spectral decomposition $\Gamma(\mathbf{k}) = \sum_{i=1}^N |v_i(\mathbf{k})\rangle\langle v_i(\mathbf{k})|$, [$N$ is the dimension size of the matrix $\Gamma(\mathbf{k})$], Eq. (25) can be rewritten as

$$\Gamma_{\mathbf{B}_1\mathbf{T}_1,\mathbf{B}_2\mathbf{T}_2} = \sum_{i=1}^N\int_\Lambda [|u_i(\mathbf{k})\rangle\langle u_i(\mathbf{k})|]_{\mathbf{B}_1\mathbf{T}_1,\mathbf{B}_2\mathbf{T}_2}, \tag{26}$$

where $|u_i(\mathbf{k})\rangle_{\mathbf{BT}} \equiv |v_i(\mathbf{k})\rangle_{\mathbf{B}}e^{i\mathbf{k}\cdot\mathbf{T}}$. Equation (26) can be written in a compact form $\Gamma = \sum_{i=1}^N\int_\Lambda |u_i(\mathbf{k})\rangle\langle u_i(\mathbf{k})|$. Substituting Eq. (26) into Eq. (24) leads to

$$\langle T^2\rangle = -\sum_{i,j}^N\int_{\Lambda^2}\mathrm{Tr}[\langle \mathrm{g}^<U_{ij}(\mathbf{k}_1,\mathbf{k}_2)\mathrm{g}^<\rangle U^\dagger_{ij}(\mathbf{k}_1,\mathbf{k}_2)], \tag{27}$$

where $U_{ij}(\mathbf{k}_1,\mathbf{k}_2) \equiv |u_i(\mathbf{k}_1)\rangle\langle u_j(\mathbf{k}_2)|$. Again, we need to compute the average over the product of two $\mathrm{g}^<$s. As we show in Appendix D, in $(\delta T)^2 = \langle T^2\rangle - \langle T\rangle^2$, the coherent part of $\langle T^2\rangle$ in Eq. (27) is exactly canceled out by the $\langle T\rangle^2$. As an important result, only the GNVC terms in $\langle T^2\rangle$ contribute to the transmission fluctuation. In other words, the fluctuation is originated from the interchannel disorder scattering. Since each vertex correction term in Eqs. (A1)–(A9) has a similar form, in the following, we still study the RR part of $\langle T^2\rangle$ as an example. The corresponding contribution to the fluctuation

is given by (see Appendix C for details)

$$\langle T^2\rangle^{(RR)}_{(\mathrm{GNVC})} = \sum_{ij}^{N}\int_{\Lambda^2}\mathrm{Tr}\left[\bar{\mathrm{g}}^R\Omega^{RR}_{ij}(\mathbf{k}_1,\mathbf{k}_2)\bar{\mathrm{g}}^R U^{\dagger}_{ij}(\mathbf{k}_1,\mathbf{k}_2)\right]$$
$$= \sum_{\mathbf{T},ij}^{N}\int_{\Lambda^2}\mathrm{Tr}\left[\bar{\mathrm{g}}^R(\mathbf{k}_1)\Omega^{RR}_{ij}(\mathbf{k}_1,\mathbf{k}_2)\bar{\mathrm{g}}^R(\mathbf{k}_2)V^{\dagger}_{ij}(\mathbf{k}_1,\mathbf{k}_2)\right], \tag{28}$$

by using $\Omega^{RR}_{ij,\mathbf{BT}}(\mathbf{k}_1,\mathbf{k}_2)=\Omega^{RR}_{ij,\mathbf{B}}(\mathbf{k}_1,\mathbf{k}_2)e^{-i(\mathbf{k}_1-\mathbf{k}_2)\mathbf{T}}$ and $\Omega^{RR}_{ij}(\mathbf{k}_1,\mathbf{k}_2)=\sum_{\mathbf{BT}}\Omega^{RR}_{ij,\mathbf{BT}}(\mathbf{k}_1,\mathbf{k}_2)$ in SSA. Here $V^{\dagger}_{ij}(\mathbf{k}_1,\mathbf{k}_2)\equiv|v_j(\mathbf{k}_2)\rangle\langle v_i(\mathbf{k}_1)|$. From the single summation over $\mathbf{T}$ in the above equation, we can see the δT scales as $\sqrt{M}$ with respect to the number of unit cells M, while the transmission coefficient and shot noise scale linearly [see Eqs. (20) and (21)]. This $\sqrt{M}$ scaling relation reflects the self-averaging effect of disorder. We obtain $\Omega^{RR}_{ij,\mathbf{B}}(\mathbf{k}_1,\mathbf{k}_2)$ by solving the linear equation,

$$\Omega^{RR}_{ij,\mathbf{B}}(\mathbf{k}_1,\mathbf{k}_2) = \langle t_{\mathbf{B}}[\bar{\mathrm{g}}^R(\mathbf{k}_1)V_{ij}(\mathbf{k}_1,\mathbf{k}_2)\bar{\mathrm{g}}^R(\mathbf{k}_2)]_{\mathbf{BB}}t_{\mathbf{B}}\rangle$$
$$-\left\langle t_{\mathbf{B}}\bar{\mathrm{g}}^R_{\mathbf{BB}}\Omega^{RR}_{ij,\mathbf{B}}(\mathbf{k}_1,\mathbf{k}_2)\bar{\mathrm{g}}^R_{\mathbf{BB}}t_{\mathbf{B}}\right\rangle$$
$$+\left\langle t_{\mathbf{B}}\sum_{\mathbf{B}'}\int_{\Lambda}\bar{\mathrm{g}}^R_{\mathbf{BB}'}(\mathbf{k})\Omega^{RR}_{ij,\mathbf{B}'}(\mathbf{k}_1,\mathbf{k}_2)\right.$$
$$\left.\times\,\bar{\mathrm{g}}^R_{\mathbf{B}'\mathbf{B}}(\mathbf{k}+\mathbf{k}_2-\mathbf{k}_1)t_{\mathbf{B}}\right\rangle, \tag{29}$$

which is also obtained by the lattice Fourier transform of Eq. (A10). The solution process for $\Omega^{XY}_{ij}(\mathbf{k}_1,\mathbf{k}_2)$ is similar to what we have described in the last subsection. After solving all the nine $\Omega^{XY}_{ij}(\mathbf{k}_1,\mathbf{k}_2)$, the transmission fluctuation can be obtained to tell the device-to-device variability from first principles.

V. NUMERICAL RESULTS AND DISCUSSIONS

Within the framework of TB-LMTO, we have implemented the generalized CPA-NVC in combination with NEGF-DFT to realize first-principles quantum transport simulation of nanoelectronics. As a numerical test, we have checked the formulation and implementation with the fluctuation dissipation theorem at the equilibrium limit by calculations with and without the GNVCs (for details, see Appendix E.) In this section, to demonstrate the effectiveness of the generalized CPA-NVC and its first-principles implementation, we calculate shot noise in a copper conductor with disordered vacancies and the fluctuation of the spin-dependent conductance through the disordered Cu/Co interface, and compare our results with other theories and experiments.

In all our electronic structure self-consistent calculations, we use the von Barth-Hedin LSDA exchange-correlation functional [36]. In shot noise simulation, we take the device model $\mathrm{Cu}/\mathrm{Cu}_{1-x}\mathrm{Va}_x/\mathrm{Cu}$ where the central region contains a different number of disordered layers with the vacancy concentration of x. In the transmission fluctuation calculation, we investigate the structure $\mathrm{Cu}/\mathrm{Cu}_{1-x}\mathrm{Co}_x/\mathrm{Co}$ where the central device region contains different disordered layers with the Co concentration of x. For both systems, we investigate the electron transport along the (111) direction in an fcc lattice structure. We use the experimental lattice constant $a = 3.615$ Å for both structures, neglecting the small lattice distortion and mismatch. For the vacancy, we represent it by a vacuum sphere without nuclear charge. For both systems, we use 50×50 k points in the whole BZ for electronic structure calculation and 60×60 k points for quantum transport simulation to obtain very well convergence. For simplicity, all our calculations are performed at zero bias, and all the transport properties are computed at the Fermi energy.

A. Shot noise for disordered Cu conductor

Theory has predicted that the Fano factor for the disordered conductor approaches a universal value 1/3 in the diffusive transport regime [37,38], and this prediction has been confirmed by experiments [12,39]. The universal 1/3 Fano factor is explained by the presence of the open transmission channels in the diffusive conductor [30]. In this subsection, we carry out the first-principles study of the transmission, shot noise, and the Fano factor in the phase-coherent copper conductors with disordered vacancies.

Figure 2 presents the averaged transmission and shot noise results for conductors with different vacancy concentrations $x = 0.025$, $x = 0.05$, and $x = 0.1$. Figures 2(a), 2(c), and 2(e) plot the transmission coefficients for the coherent part, vertex correction part, and the total. We can see for the three different vacancy concentrations, the total transmissions (in black square) all decrease with the increase of length, and we have checked that, after a certain length, the resistance R that is proportional to $1/T$ becomes linearly dependent on the length L, obeying the Ohms law. It should be noted that this correct behavior can only be obtained by including the contribution of the vertex correction, which accounts for the interchannel scattering. From Figs. 2(a), 2(c), and 2(e), it is clearly seen that, as the length increases, the interchannel scattering, accounted for by the vertex correction part, becomes more and more important, and finally dominate the total transmission for all the three concentrations investigated here, while the coherent parts all behave oppositely, quickly decaying to very small value. For example, at the length $L = 50$ layers, vertex correction is 0.346 for $x = 0.025$, 0.311 for $x = 0.05$ and 0.206 for $x = 0.1$ while the corresponding total transmission is 0.459, 0.331, 0.207 for the respective three concentrations.

Figures 2(b), 2(d), and 2(f) present the shot noise results: The GNVCs (absolute value) are shown in the purple triangle, without GNVCs shown in the red circle, and the total in the black square. Here, "without GNVCs" means we include the vertex correction in the transmission coefficient and only use the coherent part of $\mathrm{Tr}[\langle\hat{T}^2\rangle]$ for the shot noise calculation. For the three concentrations, all the total shot noises quickly increase from zero to a maximum when the transmission is close to 0.5 and then start to decrease as the number of disordered layers further increases. For the perfect copper conductor, shot noise equals zero because of the zero reflection without scattering. The presence of disorder scattering gives rise to the back scattering, thus giving the reflection and the

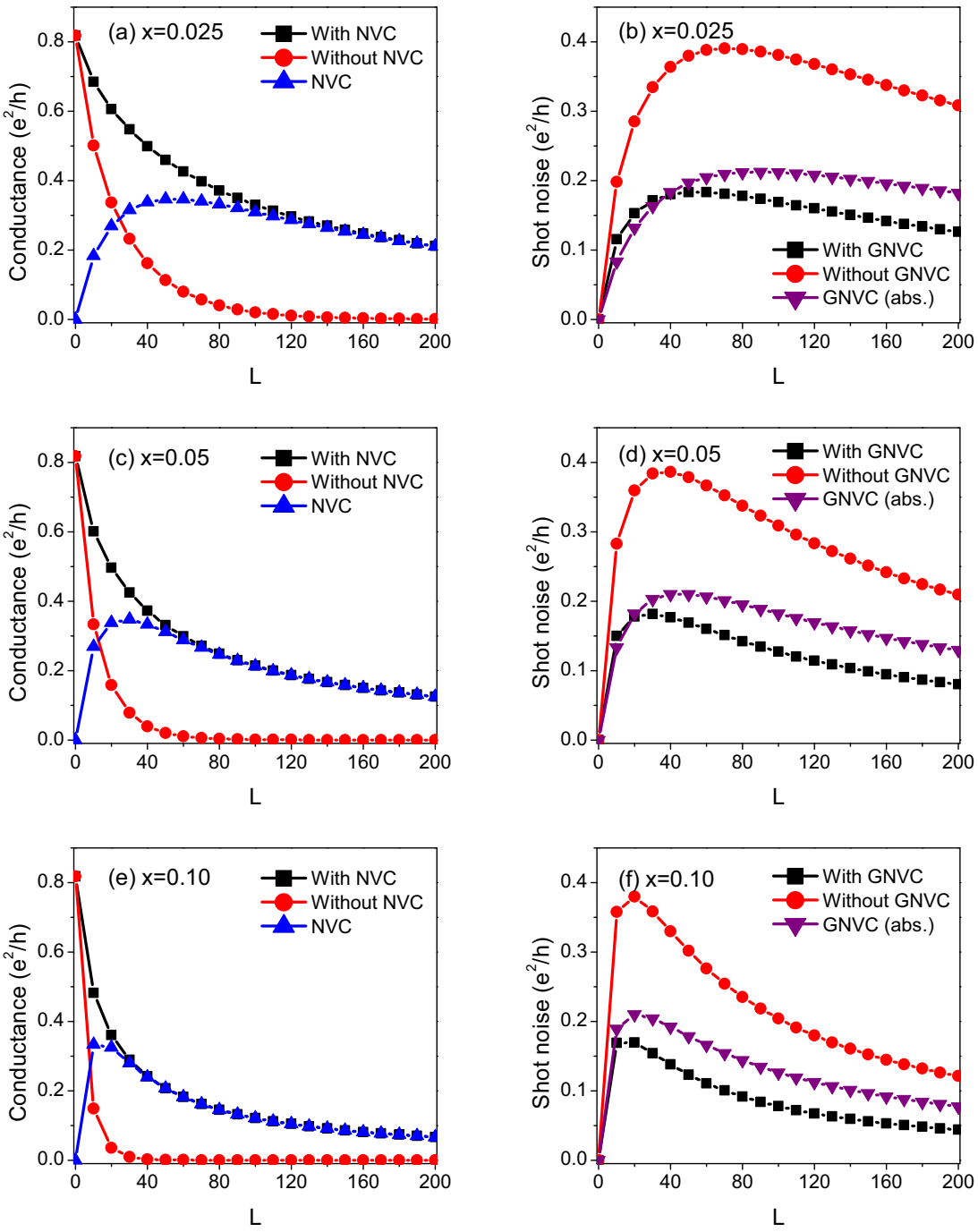

FIG. 2. Transmission and shot noise versus the length of disordered layers L (atomic layer) for $Cu/Cu_{1-x}Va_x/Cu$. (Left column) The averaged transmission $\mathrm{Tr}[\langle\hat{T}\rangle]$. (a), (c), and (e) are for $x = 0.025$, $x = 0.05$, and $x = 0.1$, respectively. (Right column) The averaged shot noise $2\mathrm{Tr}[\langle\hat{T}\rangle - \langle\hat{T}^2\rangle]$. (b), (d), and (f) are for $x = 0.025$, $x = 0.05$, and $x = 0.1$, respectively. (Note that the GNVC contribution is negative and its absolute value is plotted.)

shot noise. In the short conductor, the shot noise increases with the increase of reflection. However as the number of disorder layers further increases, the transmission decreases to a point that the shot noise starts to decrease. Similar to the transmission coefficients, we can see the GNVCs play important roles in the calculation of the shot noise. For example, the GNVC results are -0.197 for $x = 0.025$, -0.210 for $x = 0.05$, and -0.178 for $x = 0.1$ while the corresponding total shot noises are 0.183, 0.169, 0.123 for the three concentrations.

In Fig. 3, we plot the Fano factor and compare it with the calculation without the GNVCs. It is clear that, with the GNVCs, all the three Fano factors are increasing and approaching but not beyond the universal value $1/3$ as the disorder length L increases, agreeing well with previous theoretical prediction [37,38] and the experimental measurements [12,39]. Without GNVCs, the Fano factor presents a wrong trend: The value increases quickly beyond $1/3$, for example, for $x = 0.1$, $L = 200$, the fano factor reaches 0.913, much

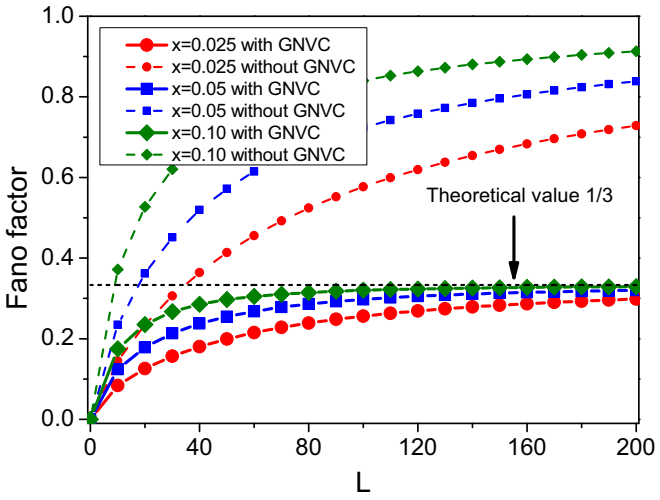

FIG. 3. Fano factor versus the number of disordered layers L (atomic layer) for $Cu/Cu_{1-x}Va_x/Cu$ structure. The red, blue, and green lines are for $x = 0.025$, $x = 0.05$, and $x = 0.1$, respectively. The horizontal dash line is the theoretical value of $1/3$ universal Fano factor for disordered conductors.

larger than $1/3$, while the result with GNVCs is 0.329, close to $1/3$. Here we want to emphasize that the inclusion of GNVCs is essential for correctly calculating the Fano factor in the disordered conductors. Therefore, it is important to effectively account for the interchannel scattering in the quantum transport simulation of the disordered nanostructures.

B. Disorders-induced conductance fluctuation for Cu/Co interface

In nanoscale devices, the random distribution of disorders can induce large fluctuation in device properties, giving rise to the large device-to-device variability. However, the quantitative study of the disorder effects on the device variability is very difficult [14]. Here, we apply the generalized CPA-NVC to study the disorder-induced device-to-device variability for spin-dependent electron transport through the Cu/Co interface along the (111) direction. For this structure, it has been experimentally shown that the variance of device resistance is very large for the minority spin channel and negligible for the majority spin channel [40]. Moreover, the first-principles supercell simulations has also shown the large variance of conductance in the minority spin channel while the majority spin almost remains unchanged when changing disorder configurations [15]. Figure 4 shows our simulation results for averaged conductance $\langle \mathcal{G} \rangle = \frac{e^2}{h}\langle T \rangle$ (the midpoint of each vertical line) and its fluctuation $\delta\mathcal{G} = \frac{e^2}{h}\delta T$ (the half width of each vertical line) for systems with single and double disorder layer(s). We can see the conductance in the minority and majority spins behaves quite differently, consistent with the experimental measurements and previous supercell simulations. First of all, it is clear that the majority spin channel has negligible fluctuation $\delta\mathcal{G}$ and almost invariant averaged conductance $\langle \mathcal{G} \rangle$ for all the different concentrations in both structures, thus presenting small device-to-device variability. In contrast, the minority spin channel shows very large

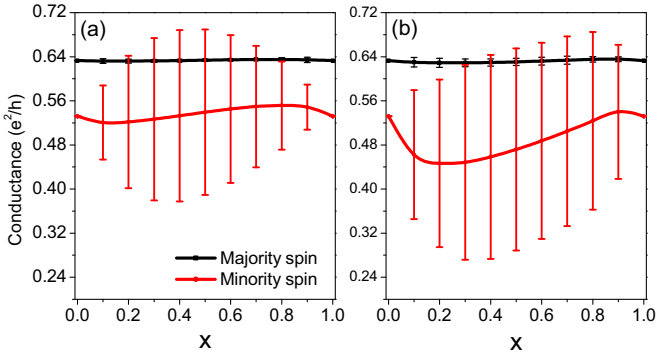

FIG. 4. Conductance and its fluctuation versus disorder concentration x for $Cu/Cu_{1-x}Co_x/Co$ structure: (a) for single disordered layer and (b) for double disordered layers. The midpoint of the vertical line is the averaged transmission coefficient $\langle T \rangle$; the half of the vertical line equals the transmission fluctuation δT.

conductance fluctuation, even comparable to the averaged $\langle \mathcal{G} \rangle$, for example, in the double disordered layer structure, $\delta\mathcal{G} = 0.185\frac{e^2}{h}$ while $\langle \mathcal{G} \rangle = 0.458\frac{e^2}{h}$ at $x = 0.4$. The fluctuation in minority spin increases quickly as the number of disorders increases. In general, the larger difference between electronic structures of the impurity and host induces the stronger impurity scattering, the larger difference between different disorder configurations, and thus gives rise to the larger resistivity and conductance fluctuation. The big difference in the transmission of the two spin channels can be attributed to the fact that the electronic structure of the Co's minority spin is very different from that of the Cu (spin unpolarized), while the majority spin of Co has the electronic structure similar to Cu, as shown in Ref. [15]. This means electrons experience much weaker scattering in the majority spin channel than in the minority spin channel, resulting in very different transmission fluctuation in the two spin channels. Without direct simulation, it is difficult to provide the quantitative or even qualitative estimate of the disorder-induced fluctuation. Here we want to emphasize again that the fluctuation is completely contributed by the GNVC terms, namely only by the interchannel disorder scattering.

VI. CONCLUSIONS

We have implemented the generalized CPA-NVC method in combination with the NEGF-DFT method within the framework of the TB-LMTO approach to realize first-principles quantum transport simulation of disordered nanoelectronics. The generalized CPA-NVC accounts for the disorder effects and the nonequilibrium statistics in the computation of electronic structure and electron transport properties. With this method, electron transport properties, such as disorder-averaged conductance, shot noise, and disorders-induced device-to-device variability (or conductance fluctuation), can all be calculated in an effective and unified way without using any phenomenological parameters. As applications, we investigated the shot noise in the disordered phase-coherent copper conductor and disorder-induced device-to-device variability in the spin-dependent transport through the Cu/Co interface. All our results agree very well with the experimental

measurements and other theories. In both applications, we have shown the generalized NVCs play a determinant role in computing the quantum transport properties of disordered nanoelectronics. Therefore, we conclude the first-principles generalized CPA-NVC method provides an effective way to treat the disorder effects on quantum transport in disordered nanoelectronics, extending the capability of first-principles simulation.

ACKNOWLEDGMENTS

Y.K. is grateful for support from the ShanghaiTech University start-up fund, "The Thousand Young Talents Plan," and Shanghai "Shuguang Plan." K.X. thanks National Basic Research Program of China (Grant No. 2012CB921304) and NNSF-China (Grants No. 61376105 and No. 21421003). We acknowledge Shanghai Supercomputer Center (SSC) for providing computational facilities.

APPENDIX A: FORMULAS OF GENERALIZED CPA-NVC METHOD

In this section, in order to make this paper self-containing, we provide the central formulas of the generalized CPA-NVC method to calculate $\langle \mathrm{g}^X c \mathrm{g}^Y\rangle$,$(X,Y = R,A,K)$, where c is a disorder-independent constant. (See more details in Ref. [18].) Before calculating the nine different $\langle \mathrm{g}^X c \mathrm{g}^Y\rangle$, we should first obtain the averaged $\bar{\mathrm{g}}^{R/A/K}$. Here $\bar{\mathrm{g}}^{R/A}$ can be obtained by the CPA and $\bar{\mathrm{g}}^K$ can be computed by including the NVC, namely $\bar{\mathrm{g}}^K = \bar{\mathrm{g}}^R(\Sigma^K + \Omega^{RA})\bar{\mathrm{g}}^A$, and Ω^{RA} is obtained by solving Eq. (A11).

After obtaining $\bar{\mathrm{g}}^{R/A/K}$, the nine different pairwise combinations $\langle \mathrm{g}^X c \mathrm{g}^Y\rangle$,$(X,Y = R,A,K)$ read

$$\langle \mathrm{g}^R c \mathrm{g}^R\rangle = \bar{\mathrm{g}}^R c \bar{\mathrm{g}}^R + \bar{\mathrm{g}}^R \Omega^{RR} \bar{\mathrm{g}}^R, \tag{A1}$$
$$\langle \mathrm{g}^R c \mathrm{g}^A\rangle = \bar{\mathrm{g}}^R c \bar{\mathrm{g}}^A + \bar{\mathrm{g}}^R \Omega^{RA} \bar{\mathrm{g}}^A, \tag{A2}$$
$$\langle \mathrm{g}^A c \mathrm{g}^R\rangle = \bar{\mathrm{g}}^A c \bar{\mathrm{g}}^R + \bar{\mathrm{g}}^A \Omega^{AR} \bar{\mathrm{g}}^R, \tag{A3}$$
$$\langle \mathrm{g}^A c \mathrm{g}^A\rangle = \bar{\mathrm{g}}^A c \bar{\mathrm{g}}^A + \bar{\mathrm{g}}^A \Omega^{AA} \bar{\mathrm{g}}^A, \tag{A4}$$
$$\langle \mathrm{g}^R c \mathrm{g}^K\rangle = \bar{\mathrm{g}}^R c \bar{\mathrm{g}}^K + \bar{\mathrm{g}}^R \Omega^{RK} \bar{\mathrm{g}}^A + \bar{\mathrm{g}}^R \Omega^{RR} \bar{\mathrm{g}}^K, \tag{A5}$$
$$\langle \mathrm{g}^A c \mathrm{g}^K\rangle = \bar{\mathrm{g}}^A c \bar{\mathrm{g}}^K + \bar{\mathrm{g}}^A \Omega^{AK} \bar{\mathrm{g}}^A + \bar{\mathrm{g}}^A \Omega^{AR} \bar{\mathrm{g}}^K, \tag{A6}$$
$$\langle \mathrm{g}^K c \mathrm{g}^R\rangle = \bar{\mathrm{g}}^K c \bar{\mathrm{g}}^R + \bar{\mathrm{g}}^R \Omega^{KR} \bar{\mathrm{g}}^R + \bar{\mathrm{g}}^K \Omega^{AR} \bar{\mathrm{g}}^R, \tag{A7}$$
$$\langle \mathrm{g}^K c \mathrm{g}^A\rangle = \bar{\mathrm{g}}^K c \bar{\mathrm{g}}^A + \bar{\mathrm{g}}^R \Omega^{KA} \bar{\mathrm{g}}^A + \bar{\mathrm{g}}^K \Omega^{AA} \bar{\mathrm{g}}^A, \tag{A8}$$
$$\langle \mathrm{g}^K c \mathrm{g}^K\rangle = \bar{\mathrm{g}}^K c \bar{\mathrm{g}}^K + \bar{\mathrm{g}}^R \Omega^{KK} \bar{\mathrm{g}}^A + \bar{\mathrm{g}}^K \Omega^{AK} \bar{\mathrm{g}}^A + \bar{\mathrm{g}}^R \Omega^{KR} \bar{\mathrm{g}}^K + \bar{\mathrm{g}}^K \Omega^{AR} \bar{\mathrm{g}}^K. \tag{A9}$$

For each $\langle \mathrm{g}^X c \mathrm{g}^Y\rangle$ above, it contains the coherent part (explicitly containing c) and the vertex correction part(s) (containing Ω). After SSA, Ω can be written as a site-diagonal quantity $\Omega = \sum_{\mathbf{R}} \Omega_{\mathbf{R}}$, which can be determined by the following nine linear equations:

$$\Omega^{RR}_{\mathbf{R}} = \langle t^R_{\mathbf{R}} [\bar{\mathrm{g}}^R c \bar{\mathrm{g}}^R]_{\mathbf{RR}} t^R_{\mathbf{R}}\rangle + \sum_{\mathbf{R}'\neq\mathbf{R}} \langle t^R_{\mathbf{R}} \bar{\mathrm{g}}^R_{\mathbf{RR}'} \Omega^{RR}_{\mathbf{R}'} \bar{\mathrm{g}}^R_{\mathbf{R}'\mathbf{R}} t^R_{\mathbf{R}}\rangle, \tag{A10}$$
$$\Omega^{RA}_{\mathbf{R}} = \langle t^R_{\mathbf{R}} [\bar{\mathrm{g}}^R c \bar{\mathrm{g}}^A]_{\mathbf{RR}} t^A_{\mathbf{R}}\rangle + \sum_{\mathbf{R}'\neq\mathbf{R}} \langle t^R_{\mathbf{R}} \bar{\mathrm{g}}^R_{\mathbf{RR}'} \Omega^{RA}_{\mathbf{R}'} \bar{\mathrm{g}}^A_{\mathbf{R}'\mathbf{R}} t^A_{\mathbf{R}}\rangle, \tag{A11}$$
$$\Omega^{AR}_{\mathbf{R}} = \langle t^A_{\mathbf{R}} [\bar{\mathrm{g}}^A c \bar{\mathrm{g}}^R]_{\mathbf{RR}} t^R_{\mathbf{R}}\rangle + \sum_{\mathbf{R}'\neq\mathbf{R}} \langle t^A_{\mathbf{R}} \bar{\mathrm{g}}^A_{\mathbf{RR}'} \Omega^{AR}_{\mathbf{R}'} \bar{\mathrm{g}}^R_{\mathbf{R}'\mathbf{R}} t^R_{\mathbf{R}}\rangle, \tag{A12}$$
$$\Omega^{AA}_{\mathbf{R}} = \langle t^A_{\mathbf{R}} [\bar{\mathrm{g}}^A c \bar{\mathrm{g}}^A]_{\mathbf{RR}} t^A_{\mathbf{R}}\rangle + \sum_{\mathbf{R}'\neq\mathbf{R}} \langle t^A_{\mathbf{R}} \bar{\mathrm{g}}^A_{\mathbf{RR}'} \Omega^{AA}_{\mathbf{R}'} \bar{\mathrm{g}}^A_{\mathbf{R}'\mathbf{R}} t^A_{\mathbf{R}}\rangle, \tag{A13}$$

$$\Omega^{RK}_{\mathbf{R}} = \langle t^R_{\mathbf{R}} [\bar{\mathrm{g}}^R c \bar{\mathrm{g}}^R]_{\mathbf{RR}} t^K_{\mathbf{R}}\rangle + \langle t^R_{\mathbf{R}} [\bar{\mathrm{g}}^R c \bar{\mathrm{g}}^K]_{\mathbf{RR}} t^A_{\mathbf{R}}\rangle + \sum_{\mathbf{R}'\neq\mathbf{R}} \left[\langle t^R_{\mathbf{R}} \bar{\mathrm{g}}^R_{\mathbf{RR}'} \Omega^{RK}_{\mathbf{R}'} \bar{\mathrm{g}}^A_{\mathbf{R}'\mathbf{R}} t^A_{\mathbf{R}}\rangle + \langle t^R_{\mathbf{R}} \bar{\mathrm{g}}^R_{\mathbf{RR}'} \Omega^{RR}_{\mathbf{R}'} \bar{\mathrm{g}}^R_{\mathbf{R}'\mathbf{R}} t^K_{\mathbf{R}}\rangle + \langle t^R_{\mathbf{R}} \bar{\mathrm{g}}^R_{\mathbf{RR}'} \Omega^{RR}_{\mathbf{R}'} \bar{\mathrm{g}}^K_{\mathbf{R}'\mathbf{R}} t^A_{\mathbf{R}}\rangle\right], \tag{A14}$$

$$\Omega^{AK}_{\mathbf{R}} = \langle t^A_{\mathbf{R}} [\bar{\mathrm{g}}^A c \bar{\mathrm{g}}^R]_{\mathbf{RR}} t^K_{\mathbf{R}}\rangle + \langle t^A_{\mathbf{R}} [\bar{\mathrm{g}}^A c \bar{\mathrm{g}}^K]_{\mathbf{RR}} t^A_{\mathbf{R}}\rangle + \sum_{\mathbf{R}'\neq\mathbf{R}} \left[\langle t^A_{\mathbf{R}} \bar{\mathrm{g}}^A_{\mathbf{RR}'} \Omega^{AK}_{\mathbf{R}'} \bar{\mathrm{g}}^A_{\mathbf{R}'\mathbf{R}} t^A_{\mathbf{R}}\rangle + \langle t^A_{\mathbf{R}} \bar{\mathrm{g}}^A_{\mathbf{RR}'} \Omega^{AR}_{\mathbf{R}'} \bar{\mathrm{g}}^R_{\mathbf{R}'\mathbf{R}} t^K_{\mathbf{R}}\rangle + \langle t^A_{\mathbf{R}} \bar{\mathrm{g}}^A_{\mathbf{RR}'} \Omega^{AR}_{\mathbf{R}'} \bar{\mathrm{g}}^K_{\mathbf{R}'\mathbf{R}} t^A_{\mathbf{R}}\rangle\right], \tag{A15}$$

$$\Omega^{KR}_{\mathbf{R}} = \langle t^K_{\mathbf{R}} [\bar{\mathrm{g}}^A c \bar{\mathrm{g}}^R]_{\mathbf{RR}} t^R_{\mathbf{R}}\rangle + \langle t^R_{\mathbf{R}} [\bar{\mathrm{g}}^K c \bar{\mathrm{g}}^R]_{\mathbf{RR}} t^R_{\mathbf{R}}\rangle + \sum_{\mathbf{R}'\neq\mathbf{R}} \left[\langle t^R_{\mathbf{R}} \bar{\mathrm{g}}^R_{\mathbf{RR}'} \Omega^{KR}_{\mathbf{R}'} \bar{\mathrm{g}}^R_{\mathbf{R}'\mathbf{R}} t^R_{\mathbf{R}}\rangle + \langle t^K_{\mathbf{R}} \bar{\mathrm{g}}^A_{\mathbf{RR}'} \Omega^{AR}_{\mathbf{R}'} \bar{\mathrm{g}}^R_{\mathbf{R}'\mathbf{R}} t^R_{\mathbf{R}}\rangle + \langle t^R_{\mathbf{R}} \bar{\mathrm{g}}^K_{\mathbf{RR}'} \Omega^{AR}_{\mathbf{R}'} \bar{\mathrm{g}}^R_{\mathbf{R}'\mathbf{R}} t^R_{\mathbf{R}}\rangle\right], \tag{A16}$$

$$\Omega^{KA}_{\mathbf{R}} = \langle t^K_{\mathbf{R}} [\bar{\mathrm{g}}^A c \bar{\mathrm{g}}^A]_{\mathbf{RR}} t^A_{\mathbf{R}}\rangle + \langle t^R_{\mathbf{R}} [\bar{\mathrm{g}}^K c \bar{\mathrm{g}}^A]_{\mathbf{RR}} t^A_{\mathbf{R}}\rangle + \sum_{\mathbf{R}'\neq\mathbf{R}} \left[\langle t^R_{\mathbf{R}} \bar{\mathrm{g}}^R_{\mathbf{RR}'} \Omega^{KA}_{\mathbf{R}'} \bar{\mathrm{g}}^A_{\mathbf{R}'\mathbf{R}} t^A_{\mathbf{R}}\rangle + \langle t^K_{\mathbf{R}} \bar{\mathrm{g}}^A_{\mathbf{RR}'} \Omega^{AA}_{\mathbf{R}'} \bar{\mathrm{g}}^A_{\mathbf{R}'\mathbf{R}} t^A_{\mathbf{R}}\rangle + \langle t^R_{\mathbf{R}} \bar{\mathrm{g}}^K_{\mathbf{RR}'} \Omega^{AA}_{\mathbf{R}'} \bar{\mathrm{g}}^A_{\mathbf{R}'\mathbf{R}} t^A_{\mathbf{R}}\rangle\right], \tag{A17}$$

$$\begin{aligned}\Omega^{KK}_{\mathbf{R}} = {} & \langle t^K_{\mathbf{R}} [\bar{\mathrm{g}}^A c \bar{\mathrm{g}}^R]_{\mathbf{RR}} t^K_{\mathbf{R}}\rangle + \langle t^K_{\mathbf{R}} [\bar{\mathrm{g}}^A c \bar{\mathrm{g}}^K]_{\mathbf{RR}} t^A_{\mathbf{R}}\rangle + \langle t^R_{\mathbf{R}} [\bar{\mathrm{g}}^K c \bar{\mathrm{g}}^R]_{\mathbf{RR}} t^K_{\mathbf{R}}\rangle + \langle t^R_{\mathbf{R}} [\bar{\mathrm{g}}^K c \bar{\mathrm{g}}^K]_{\mathbf{RR}} t^A_{\mathbf{R}}\rangle + \sum_{\mathbf{R}'\neq\mathbf{R}} \Big[\langle t^R_{\mathbf{R}} \bar{\mathrm{g}}^R_{\mathbf{RR}'} \Omega^{KK}_{\mathbf{R}'} \bar{\mathrm{g}}^A_{\mathbf{R}'\mathbf{R}} t^A_{\mathbf{R}}\rangle \\ & + \langle t^K_{\mathbf{R}} \bar{\mathrm{g}}^A_{\mathbf{RR}'} \Omega^{AK}_{\mathbf{R}'} \bar{\mathrm{g}}^A_{\mathbf{R}'\mathbf{R}} t^A_{\mathbf{R}}\rangle + \langle t^R_{\mathbf{R}} \bar{\mathrm{g}}^R_{\mathbf{RR}'} \Omega^{KR}_{\mathbf{R}'} \bar{\mathrm{g}}^R_{\mathbf{R}'\mathbf{R}} t^K_{\mathbf{R}}\rangle + \langle t^K_{\mathbf{R}} \bar{\mathrm{g}}^A_{\mathbf{RR}'} \Omega^{AR}_{\mathbf{R}'} \bar{\mathrm{g}}^R_{\mathbf{R}'\mathbf{R}} t^K_{\mathbf{R}}\rangle \\ & + \langle t^R_{\mathbf{R}} \bar{\mathrm{g}}^K_{\mathbf{RR}'} \Omega^{AR}_{\mathbf{R}'} \bar{\mathrm{g}}^R_{\mathbf{R}'\mathbf{R}} t^K_{\mathbf{R}}\rangle + \langle t^R_{\mathbf{R}} \bar{\mathrm{g}}^R_{\mathbf{RR}'} \Omega^{KR}_{\mathbf{R}'} \bar{\mathrm{g}}^K_{\mathbf{R}'\mathbf{R}} t^A_{\mathbf{R}}\rangle + \langle t^K_{\mathbf{R}} \bar{\mathrm{g}}^A_{\mathbf{RR}'} \Omega^{AR}_{\mathbf{R}'} \bar{\mathrm{g}}^K_{\mathbf{R}'\mathbf{R}} t^A_{\mathbf{R}}\rangle + \langle t^R_{\mathbf{R}} \bar{\mathrm{g}}^K_{\mathbf{RR}'} \Omega^{AR}_{\mathbf{R}'} \bar{\mathrm{g}}^K_{\mathbf{R}'\mathbf{R}} t^A_{\mathbf{R}}\rangle\Big].\end{aligned} \tag{A18}$$

These nine equations are decoupled if we solve them from top to down, because each time we only have one unknown Ω to solve. As we know [18], any averaged two-real-time-GF correlators can easily be obtained by the linear combination of $\langle g^X c g^Y\rangle, (X,Y = R,A,K)$ in Eqs. (A1)–(A9), for example,

$$\langle g^< c g^<\rangle = \tfrac{1}{4}[\langle g^R c g^R\rangle - \langle g^R c g^A\rangle - \langle g^R c g^K\rangle - \langle g^A c g^R\rangle + \langle g^A c g^A\rangle + \langle g^A c g^K\rangle - \langle g^K c g^R\rangle + \langle g^K c g^A\rangle + \langle g^K c g^K\rangle]. \quad \text{(A19)}$$

APPENDIX B: DERIVATION OF EQS. (22) AND (23)

Equation (22) is derived by the lattice Fourier transform of Eq. (21). To do this, we first consider the first term of Eq. (21) and obtain

$$\begin{aligned}\mathrm{Tr}[\bar{g}^R\Gamma_R\bar{g}^R\Gamma_R] &= \sum_{\mathbf{B}_1\mathbf{T}_1}\sum_{\mathbf{B}_2\mathbf{T}_2}\sum_{\mathbf{B}_3\mathbf{T}_3}\sum_{\mathbf{B}_4\mathbf{T}_4}\bar{g}^R_{\mathbf{B}_1\mathbf{T}_1,\mathbf{B}_2\mathbf{T}_2}\Gamma_{R,\mathbf{B}_2\mathbf{T}_2,\mathbf{B}_3\mathbf{T}_3}\bar{g}^R_{\mathbf{B}_3\mathbf{T}_3,\mathbf{B}_4\mathbf{T}_4}\Gamma_{R,\mathbf{B}_4\mathbf{T}_4,\mathbf{B}_1\mathbf{T}_1}\\ &= \sum_{\mathbf{T}_4}\int_{\Lambda^4}\mathrm{Tr}[\bar{g}^R(\mathbf{k}_1)\Gamma_R(\mathbf{k}_2)\bar{g}^R(\mathbf{k}_3)\Gamma_R(\mathbf{k}_4)]\sum_{\mathbf{T}_1}e^{-i(\mathbf{k}_4-\mathbf{k}_1)\cdot\mathbf{T}_1}\sum_{\mathbf{T}_2}e^{-i(\mathbf{k}_1-\mathbf{k}_2)\cdot\mathbf{T}_2}\sum_{\mathbf{T}_3}e^{-i(\mathbf{k}_2-\mathbf{k}_3)\cdot\mathbf{T}_3}e^{-i(\mathbf{k}_3-\mathbf{k}_4)\cdot\mathbf{T}_4}\\ &= \sum_{\mathbf{T}}\int_{\Lambda}\mathrm{Tr}[\bar{g}^R(\mathbf{k})\Gamma_R(\mathbf{k})\bar{g}^R(\mathbf{k})\Gamma_R(\mathbf{k})], \end{aligned} \quad \text{(B1)}$$

where we have used identity $\sum_{\mathbf{T}}e^{-i\mathbf{k}\cdot\mathbf{T}} = \delta(\mathbf{k})$. The second term of Eq. (21) can be obtained similarly. Note that Ω is a site-diagonal quantity $\Omega = \sum_{\mathbf{BT}}\Omega_{\mathbf{BT}}$, and $\Omega_{\mathbf{BT}} = \Omega_{\mathbf{B}}$. By using these facts, we can easily obtain Eq. (21). Equation (23) is derived from the lattice Fourier transform of Eq. (A10) [c in Eq. (A10) is replaced with Γ_R here], we first rewrite

$$\Omega^{RR}_{\mathbf{B}} = \langle t^R_{\mathbf{B}}[\bar{g}^R\Gamma_R\bar{g}^R]_{\mathbf{BB}}t^R_{\mathbf{B}}\rangle - \langle t^R_{\mathbf{B}}\bar{g}^R_{\mathbf{BB}}\Omega^{RR}_{\mathbf{B}}\bar{g}^R_{\mathbf{BB}}t^R_{\mathbf{B}}\rangle + \sum_{\mathbf{B}'\mathbf{T}'}\langle t^R_{\mathbf{B}}\bar{g}^R_{\mathbf{B},\mathbf{B}'\mathbf{T}'}\Omega^{RR}_{\mathbf{B}'\mathbf{T}'}\bar{g}^R_{\mathbf{B}'\mathbf{T}',\mathbf{B}}t^R_{\mathbf{B}}\rangle. \quad \text{(B2)}$$

By applying the lattice Fourier transform and using $\Omega_{\mathbf{B}'\mathbf{T}'} = \Omega_{\mathbf{B}'}$, we can obtain Eq. (23) from the above equation.

APPENDIX C: DERIVATION OF EQS. (28) AND (29)

Equation (28) is derived from the vertex correction term in Eq. (A1). To see the details, we have

$$\begin{aligned}\langle T^2\rangle^{(RR)}_{(\mathrm{GNVC})} &= \sum_{ij}^{N}\int_{\Lambda^2}\mathrm{Tr}\big[\bar{g}^R\Omega^{RR}_{ij}(\mathbf{k}_1,\mathbf{k}_2)\bar{g}^R U^\dagger_{ij}(\mathbf{k}_1,\mathbf{k}_2)\big]\\ &= \sum_{ij}^{N}\int_{\Lambda^2}\sum_{\mathbf{B}_1\mathbf{T}_1}\sum_{\mathbf{B}_2\mathbf{T}_2}\sum_{\mathbf{B}_3\mathbf{T}_3}\bar{g}^R_{\mathbf{B}_1\mathbf{T}_1,\mathbf{B}_2\mathbf{T}_2}\Omega^{RR}_{ij,\mathbf{B}_2\mathbf{T}_2}(\mathbf{k}_1,\mathbf{k}_2)\bar{g}^R_{\mathbf{B}_2\mathbf{T}_2,\mathbf{B}_3\mathbf{T}_3}[U^\dagger_{ij}(\mathbf{k}_1,\mathbf{k}_2)]_{\mathbf{B}_3\mathbf{T}_3,\mathbf{B}_1\mathbf{T}_1}\\ &= \sum_{ij}^{N}\int_{\Lambda^2}\sum_{\mathbf{B}_1\mathbf{T}_1}\sum_{\mathbf{B}_2\mathbf{T}_2}\sum_{\mathbf{B}_3\mathbf{T}_3}\bar{g}^R_{\mathbf{B}_1\mathbf{B}_2}(\mathbf{k}_3)\Omega^{RR}_{ij,\mathbf{B}_2}(\mathbf{k}_1,\mathbf{k}_2)\bar{g}^R_{\mathbf{B}_2\mathbf{B}_3}(\mathbf{k}_4)[V^\dagger_{ij}(\mathbf{k}_1,\mathbf{k}_2)]_{\mathbf{B}_3\mathbf{B}_1}e^{-i(\mathbf{k}_1-\mathbf{k}_3)\cdot\mathbf{T}_1}e^{-i(\mathbf{k}_3-\mathbf{k}_4+\theta)\cdot\mathbf{T}_2}e^{-i(\mathbf{k}_4-\mathbf{k}_2)\cdot\mathbf{T}_3}\\ &= \sum_{ij}^{N}\int_{\Lambda^2}\sum_{\mathbf{T}_2}\mathrm{Tr}\big[\bar{g}^R(\mathbf{k}_1)\Omega^{RR}_{ij}(\mathbf{k}_1,\mathbf{k}_2)\bar{g}^R(\mathbf{k}_2)V^\dagger_{ij}(\mathbf{k}_1,\mathbf{k}_2)\big]e^{-i(\mathbf{k}_1-\mathbf{k}_2+\theta)\cdot\mathbf{T}_2}, \end{aligned} \quad \text{(C1)}$$

where we have supposed $\Omega^{RR}_{ij,\mathbf{BT}}(\mathbf{k}_1,\mathbf{k}_2) = \Omega^{RR}_{ij,\mathbf{B}}(\mathbf{k}_1,\mathbf{k}_2)e^{-i\theta\cdot\mathbf{T}}$. Because each unit cell must provide the same contribution to the fluctuation, $\theta = \mathbf{k}_2 - \mathbf{k}_1$ is required, and finally we obtain Eq. (28).

By replacing c with $U_{ij}(\mathbf{k}_1,\mathbf{k}_2)$ in Eq. (A10), Eq. (29) can be obtained by the lattice Fourier transform with the relation $\Omega^{RR}_{ij,\mathbf{BT}}(\mathbf{k}_1,\mathbf{k}_2) = \Omega^{RR}_{ij,\mathbf{B}}(\mathbf{k}_1,\mathbf{k}_2)e^{-i(\mathbf{k}_2-\mathbf{k}_1)\cdot\mathbf{T}}$ and $[U_{ij}(\mathbf{k}_1,\mathbf{k}_2)]_{\mathbf{BT},\mathbf{B}'\mathbf{T}'} = [V_{ij}(\mathbf{k}_1,\mathbf{k}_2)]_{\mathbf{B},\mathbf{B}'}e^{-i(\mathbf{k}_2\mathbf{T}'-\mathbf{k}_1\mathbf{T})}$.

APPENDIX D: MORE ABOUT TRANSMISSION FLUCTUATION

The disorders-induced transmission fluctuation is entirely contributed by GNVCs. To see this fact more clearly, from the definition of the transmission coefficient we have

$$\langle T\rangle = -i\sum_{i=1}^{N}\int_{\Lambda}\mathrm{Tr}[\bar{g}^<|u_i(\mathbf{k})\rangle\langle u_i(\mathbf{k})|], \quad \text{(D1)}$$

and therefore

$$\langle T\rangle^2 = -\sum_{ij}^{N}\int_{\Lambda^2}\mathrm{Tr}[\bar{g}^< U_{ij}(\mathbf{k}_1,\mathbf{k}_2)\bar{g}^< U^\dagger_{ij}(\mathbf{k}_1,\mathbf{k}_2)]. \quad \text{(D2)}$$

Comparing with Eq. (27), we can find $\langle T\rangle^2$ is exactly the coherent part of $\langle T^2\rangle$, which is canceled out in the calculation

of δT. Therefore, in order to obtain δT, we only need to calculate the GNVC part of $\langle T^2 \rangle$.

APPENDIX E: TEST THE GENERALIZED NVCS WITH FLUCTUATION DISSIPATION THEOREM

The fluctuation dissipation theorem says that for a system at equilibrium, the Green's functions satisfy

$$\mathrm{g}^{\alpha,<} = \mathrm{g}^{\alpha,A} - \mathrm{g}^{\alpha,R}, \tag{E1}$$

which can be used as a strong test to our implementation. For example, to test the correctness of GNVC terms in the quantity $\langle \mathrm{g}^{\alpha,<} c \mathrm{g}^{\alpha,<} \rangle$, we insert Eq. (E1) into it and get

$$\langle \mathrm{g}^{\alpha,<} c \mathrm{g}^{\alpha,<} \rangle = \langle \mathrm{g}^{\alpha,A} c \mathrm{g}^{\alpha,A} \rangle - \langle \mathrm{g}^{\alpha,A} c \mathrm{g}^{\alpha,R} \rangle - \langle \mathrm{g}^{\alpha,R} c \mathrm{g}^{\alpha,A} \rangle + \langle \mathrm{g}^{\alpha,R} c \mathrm{g}^{\alpha,R} \rangle. \tag{E2}$$

The left-hand side of Eq. (E2) can be calculated by including all the GNVC terms in Eqs. (A1)–(A9), while the right-hand side terms only require the simplest vertex corrections in Eqs. (A1)–(A4). In our implementation, we have tested the fluctuation dissipation theorem in both the disordered copper conductor investigated in Sec. V A and the disordered Cu/Co interface discussed in Sec. V B. In both cases, the results on the left-hand side and right-hand side in Eq. (E2) are essentially the same, providing a rigorous test to our numerical implementations.

[1] S. Datta, *Electronic Transport in Mesoscopic Systems* (Cambridge University Press, Cambridge, 1997).
[2] A. Asenov, IEEE Trans. Electron Devices **45**, 2505 (1998).
[3] P. Hohenberg and W. Kohn, Phys. Rev. **136**, B864 (1964); W. Kohn and L. J. Sham, *ibid.* **140**, A1133 (1965); R. G. Parr and W. Yang, *Density-Functional Theory of Atoms and Molecules* (Oxford University Press, Oxford, 1989), Vol. 16.
[4] H. Haug, A.-P. Jauho, and M. Cardona, *Quantum Kinetics in Transport and Optics of Semiconductors* (Springer, Berlin, 2008), Vol. 2.
[5] L. Keldysh, Sov. Phys. JETP **20**, 1018 (1965).
[6] J. Taylor, H. Guo, and J. Wang, Phys. Rev. B **63**, 121104 (2001); **63**, 245407 (2001).
[7] Y. Xue, S. Datta, and M. A. Ratner, Chem. Phys. **281**, 151 (2002); W. Lu, V. Meunier, and J. Bernholc, Phys. Rev. Lett. **95**, 206805 (2005); M. Brandbyge, J.-L. Mozos, P. Ordejón, J. Taylor, and K. Stokbro, Phys. Rev. B **65**, 165401 (2002).
[8] S. V. Faleev, F. Léonard, D. A. Stewart, and M. van Schilfgaarde, Phys. Rev. B **71**, 195422 (2005).
[9] Applications of the CPA-NVC: Y. Ke, K. Xia, and H. Guo, Phys. Rev. Lett. **105**, 236801 (2010); Y. Ke, F. Zahid, V. Timoshevskii, K. Xia, D. Gall, and H. Guo, Phys. Rev. B **79**, 155406 (2009); F. Zahid, Y. Ke, D. Gall, and H. Guo, *ibid.* **81**, 045406 (2010); X. Jia, K. Xia, Y. Ke, and H. Guo, *ibid.* **84**, 014401 (2011); Z. Wang, Y. Ke, D. Liu, H. Guo, and K. H. Bevan, Appl. Phys. Lett. **101**, 093102 (2012); C. Franz, M. Czerner, and C. Heiliger, J. Phys.: Condens. Matter **25**, 425301 (2013); C. Heiliger, C. Franz, and M. Czerner, Phys. Rev. B **87**, 224412 (2013); C. Franz, M. Czerner, and C. Heiliger, *ibid.* **88**, 094421 (2013).
[10] Y. Zhang, L. Meng, C. Yam, and G. Chen, J. Phys. Chem. Lett. **5**, 1272 (2014).
[11] X. Jehl, M. Sanquer, R. Calemczuk, and D. Mailly, Nature (London) **405**, 50 (2000).
[12] A. H. Steinbach, J. M. Martinis, and M. H. Devoret, Phys. Rev. Lett. **76**, 3806 (1996).
[13] O. Agam, I. Aleiner, and A. Larkin, Phys. Rev. Lett. **85**, 3153 (2000).
[14] Y. Zhu, L. Liu, and H. Guo, Phys. Rev. B **88**, 085420 (2013); J. N. Zhuang and J. Wang, J. Appl. Phys. **114**, 063708 (2013).
[15] K. Xia, M. Zwierzycki, M. Talanana, P. J. Kelly, and G. E. W. Bauer, Phys. Rev. B **73**, 064420 (2006).
[16] Q. Shi, H. Guo, Y. Zhu, and L. Liu, Phys. Rev. Appl. **3**, 064008 (2015).
[17] K. Liu, K. Xia, and G. E. W. Bauer, Phys. Rev. B **86**, 020408 (2012).
[18] J. Yan and Y. Ke, Phys. Rev. B **94**, 045424 (2016).
[19] I. Turek, V. Drchal, J. Kudrnovský, M. Sob, and P. Weinberger, *Electronic Structure of Disordered Alloys, Surfaces and Interfaces* (Springer Science & Business Media, Berlin/Heidelberg, 2013).
[20] O. K. Andersen and O. Jepsen, Phys. Rev. Lett. **53**, 2571 (1984).
[21] O. K. Andersen, Z. Pawlowska, and O. Jepsen, Phys. Rev. B **34**, 5253 (1986).
[22] J. Schwinger, J. Math. Phys. **2**, 407 (1961).
[23] L. P. Kadanoff and G. A. Baym, *Quantum Statistical Mechanics* (Benjamin, New York, 1962).
[24] J. Rammer and H. Smith, Rev. Mod. Phys. **58**, 323 (1986).
[25] A. Kamenev, *Field Theory of Non-Equilibrium Systems* (Cambridge University Press, Cambridge, 2011).
[26] L. D. Landau, E. Lifshitz, and L. Pitaevskij, *Course of Theoretical Physics*, Physical Kinetics (Oxford University Press, Oxford, 1981), Vol. 10.
[27] Y. Ke, K. Xia, and H. Guo, Phys. Rev. Lett. **100**, 166805 (2008).
[28] G. D. Mahan, *Many-Particle Physics* (Springer Science & Business Media, Berlin/Heidelberg, 2013).
[29] Y. Wei, B. Wang, J. Wang, and H. Guo, Phys. Rev. B **60**, 16900 (1999).
[30] Y. Blanter and M. Bttiker, Phys. Rep. **336**, 1 (2000); C. Beenakker and C. Schönenberger, Phys. Today **56**(3), 37 (2003).
[31] W. Schottky, Ann. Phys. **362**, 541 (1918).
[32] P. Soven, Phys. Rev. **156**, 809 (1967).
[33] D. W. Taylor, Phys. Rev. **156**, 1017 (1967).
[34] B. Velický, S. Kirkpatrick, and H. Ehrenreich, Phys. Rev. **175**, 747 (1968).
[35] B. Velický, Phys. Rev. **184**, 614 (1969).
[36] U. von Barth and L. Hedin, J. Phys. C **5**, 1629 (1972).
[37] C. W. J. Beenakker and M. Büttiker, Phys. Rev. B **46**, 1889 (1992).
[38] K. Nagaev, Phys. Lett. A **169**, 103 (1992).
[39] R. J. Schoelkopf, P. J. Burke, A. A. Kozhevnikov, D. E. Prober, and M. J. Rooks, Phys. Rev. Lett. **78**, 3370 (1997).
[40] J. Bass and W. P. Pratt, Jr., J. Magn. Magn. Mater. **200**, 274 (1999).